Geomechanics and Engineering, *Vol. 18, No. 5 (2019) 481-492*
DOI: https://doi.org/10.12989/gae.2019.18.5.481

Experimental study of rockburst under true-triaxial gradient loading conditions

Xiqi Liu[1a], Yuanyou Xia*[1], Manqing Lin[2b] and Mahfoud Benzerzour[3c]

[1]School of Civil Engineering and Architecture, Wuhan University of Technology, Wuhan 430070, China
[2]School of Xingfa Mining Engineering, Wuhan Institute of Technology, Wuhan 430062, China
[3]Institute Mines-Telecom Lille Douai, Douai 59500, France

(Received March 4, 2019, Revised June 4, 2019, Accepted July 15, 2019)

Abstract. Due to the underground openings, the tangentially concentrated stress of the tunnel remains larger at excavation boundary and decreases toward the interior of the surrounding rock with a certain gradient. In order to study the effect of different gradient stress on rockburst, the true-triaxial gradient and hydraulic-pneumatic combined test apparatus were carried out to simulate the rockburst processes. Under the different gradient stress conditions, the rock-like specimen (gypsum) was tested independently through three principal stress directions loading--fast unloading of single surface--top gradient and hydraulic-pneumatic combined loading, which systematically analyzed the macro-mesoscopic damage phenomena, force characteristics and acoustic emission (AE) signals of the specimen during rockburst. The experimental results indicated that the rockburst test under the gradient and hydraulic-pneumatic combined loading conditions could perfectly reflect the rockburst processes and their stress characteristics; Relatively high stress loading could cause specimen failure, but could not determine its mode. The rockburst under the action of gradient stress suggested that the failure mode of specimen mainly depended on the stress gradient. When the stress gradient was lower, progressive and static spalling failure occured and the rockburst grades were relatively slight. On the other hand, shear fractures occurred in rockbursts accounted for increasingly large proportion as the stress gradient increased and the rockburst occurred more intensely and suddenly, the progressive failure process became unconspicuous, and the rockburst grades were moderate or even stronger.

Keywords: rockburst; failure modes; true-triaxial; stress gradient; hydraulic-pneumatic combined loading

1. Introduction

With the development of transportation, water conservancy, nuclear waste storage and other projects proceeding to deep rocks in the world, the mechanical behavior under high in-situ stress and the complex geological structure of hard rocks lead to complicated failure of surrounding rock masses in the excavation process (Jiří 2017, Fuławka *et al.* 2018, Tan *et al.* 2018). A rockburst is a destructive and common form of disaster in underground engineering. Rockbursts are mainly divided into two types (Cai and Champaigne 2012, Yan *et al.* 2015), namely, progressive failure (i.e., spalling or slabbing failure) which is often accompanied by progressive generation of surface parallel fractures without ejection, as presented in Fig. 1(a), or unstable manner, which often accumulates elastic strain energy, ejects with falling blocks and develops dome-like or wedge burst, as illustrated in Fig. 1(b). Different types of rockburst result in various disaster characteristics, which usually appears to be sudden and often poses an underground safety hazard to workers and mining equipment (Mazaira and Konicek 2015, Stacey 2016, Song *et al.* 2017). Therefore, gaining deep insight into the rockburst phenomena is particularly important to safe underground construction at depth.

(a) Spalling failure (b) Shear failure

Fig. 1 Different failure modes of rockburst (Bayu Tunnel at Lalin Railway in China)

Rockbursts are mainly conditioned by two factors, namely rock mass conditions and stress field conditions (Wang 2018). The vast majority of deep rock masses are hard-brittle ones which meet the requirements of lithological conditions for rockbursts. Therefore, it is

*Corresponding author, Professor
E-mail: xiayy1965@whut.edu.cn
[a]Ph.D. Student
E-mail: liuxx142857@163.com
[b]Associate Professor
E-mail: manqing_lin@foxmail.com
[c]Professor
E-mail: mahfoud.benzerzour@imt-lille-douai.fr

ISSN: 2005-307X (Print), 2092-6219 (Online)

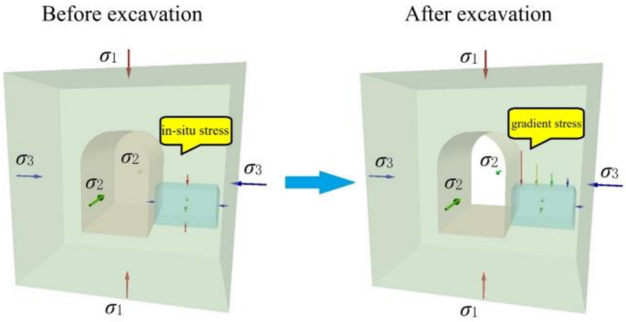

Fig. 2 The gradient distribution of tangential stress in surrounding rock

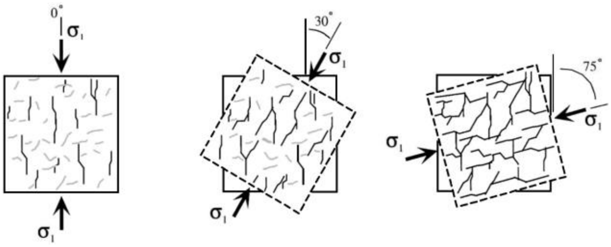

Fig. 3 Effects of the principal stress direction on fracture development (Diederichs *et al.* 2004)

important to study the stress paths during the tunnel excavations for the further comprehension of rockburst phenomena (Gattinoni *et al.* 2014). Thereby, a rockburst study should deal with the basic stress conditions and loading paths, which is characterized by unloading of radial stress and an increase of tangential stress as well as the approximately unchanged intermediate stress (Manouchehrian 2016). Therefore, one free face loading tests under true-triaxial condition were performed to simulate the strainburst using a true-triaxial rockburst testing apparatus. Gong *et al.* (2012) analyzed two brittle failure modes of the surrounding rocks of the JinpingII and reproduced the spalling phenomena of the rock through the true-triaxial tests. He *et al.* (2012, 2015) reproduced the whole process of rockburst with the independently-developed true-triaxial test system, detailedly discussed the acoustic emission (AE) characteristics of the whole process of rockbursts. Qiu *et al.* (2014) reconstructed the occurrence of the spalling with the true-triaxial test and explored its mechanical mechanism of instability. Akdag *et al.* (2018) investigated the effects of thermal damage to the strainburst characteristics of brittle rocks under the true-triaxial loading-unloading conditions, and systematically explored the evolution of acoustic emission (AE) due to thermal damage influence on strainburst. Thomas B *et al.* (2018) studied the damage behavior of deep rock masses and simulated their stress state during rockburst by using a new rockburst test instrument. Furthermore, Bruning *et al.* (2018) investigated the characteristics of the stress and the relationship between deviatoric stress and in-situ pressure/depth, which provides valuable information about the necessary conditions for rockburst in deep mining.

The aforementioned tests are of great significance for the study of rockburst mechanisms. However, due to the complexity of geology and the triggering conditions in situ, it is widely accepted that, in the current rockburst tests, the small-volume specimen suffers uniform loading, which is different from the gradient stress distribution of the surrounding rock in the disturbed zone during the underground excavations. An open of free boundary changes the stress state of the rock masses near the excavated boundary. The tangential stress increases gradually with certain gradient, the radial stress decreases rapidly, and the axis stress remains unchanged, as in Fig. 2.

The mechanical behavior of rock depends on the change of stress state, and the force is closely and correspondingly related to the deformation and failure of surrounding rock (Thomas *et al.* 2019). Thus, rockburst is closely related to the stress state of the rock masses near the excavated boundary. The generation, expansion, and penetration of cracks in rock masses always occur along the direction of the maximum principal stress (Germanovish and Dyskin 2000). Under the condition of uniform loading, the cracks extend parallel to the unloading surface, spalling rockburst happened most often. However, The gradient distributions of the tangential stress in the surrounding rock can generate shear stress among the surrounding rock mass units. This leads to deflections of the stress principal axes. The rotations of the stress principal axes are the controlling factors of the crack propagation directions and affect failure mechanisms of the surrounding rock masses, as shown in Fig. 3. Furthermore, the ratio of the maximum stress at excavation boundary to the uniaxial compressive strength ($\sigma_{\theta\max}/\sigma_c$) is between 0.3 and 0.7 (Roohollah and Abbas 2018). This indicates that, as the rockburst occurs, the intact rock masses around the rockburst area which are in the state of elasticity can release strain energy due to unloading and are equivalent to a flexible loading system (Gu *et al.* 2014, Thomas *et al.* 2016). However, most of the traditional rockburst test equipment adopted to the hydraulic rigid loading system. During the failure processes of the specimens, the load pressure drop was unable to be compensated, so the rockburst ejection phenomena were difficult to be reproduced.

To solve the problems mentioned above, in this paper, a novel experimental technique was proposed. It employed gradient stress loading path to reproduce the circumstances of the occurrence of the rockburst and four rockburst tests under different gradient stress paths respectively were conducted on specimens (400 mm×600 mm×1,000 mm) using a true-triaxial gradient and hydraulic-pneumatic combined text apparatus. Based on that, we analyzed the effects of gradient stress on the rockburst. Furthermore, we can analyze the rockburst mechanism and identify the factors that influence rockburst intensity. The experimental results will potentially be helpful to further elucidating the inoculation and generation mechanisms of strainburst phenomena.

2. The failure mechanism of rockburst in intact surrounding rock masses

In order to study the influence of different loading path on the rockburst failure processes of intact surrounding rock, studies on rockbursts failure modes of intact

Table 1 Rockbursts occurred in Bayu Tunnel at Lalin Railway in China and the corresponding failure modes

Typical rockburst phenomena	Scene photos of rockbursts	Failure Modes (Li *et al*. 2017)
In June, 2018, rockburst had mainly occurred on the right side of DK200+091in the form of the spalling of the rock slabs, without obvious throwing phenomena. The harm to the projects can not be ignored as the damage range is relatively large. **(Slight rockburst)**		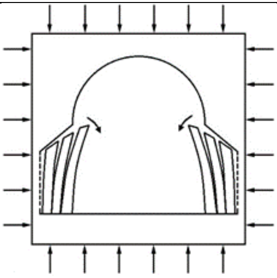 **(Tensile fractures)**
On September 11, 2016, a large number of rock plates burst off or ejected at the DK193+566, and the blasting pit was a pan-shaped cavity with an influence depth greater than 0.5 m. It had mainly occurred in the form of the throwing of the lenticular rock masses with sharp edges. **(moderate rockburst)**	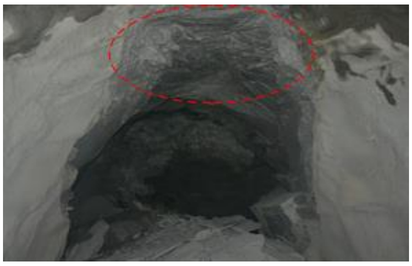	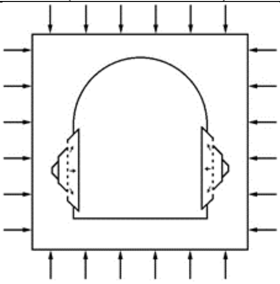 **(Tensile-shear fractures)**
On December 11, 2016, a large piece of the surrounding rock masses had continuously burst at the vault of DK195+443 and a large volume of rock had appeared to be ejected, forming a V-shaped shear rock blasting pit. **(strong rock-burst)**		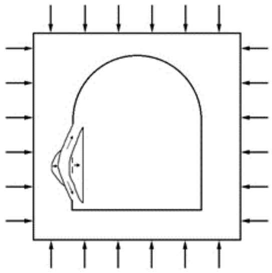 **(Shear fractures)**

surrounding rock were conducted in Bayu tunnel of Lalin railway, as shown in Table 1.

According to the rockburst phenomena of intact surrounding rock masses in the table, based on different mechanical mechanisms of surrounding rock masses, they can be fallen into three categories (Li *et al*. 2017):

(1) Tensile fractures (sheeting or bed spalling): Rock masses surrounding an underground opening peel off layer-by-layer, and along the huge rock plate parallels to excavation surface, producing sheets or plates. The failure plane is usually flat, exhibiting conchoidalradial patterns of fracture.

(2) Tensile-shear fractures (buckling break): After excavation in highly stressed rock masses, tensile-shear fractures develop, and progressively expand towards both sides of the free surface, resulting in wedge burst. A moderate grade of rockburst occurs with large steps. In general, the failure plane is relatively flat in central parts and jagged along edges.

(3) Shear fractures (dome-like or wedge burst): Surrounding rock masses fail via shear fracture because the local stresses concentrate, which followed by ejection phenomena. The failure plane is dome-like or forms wedges by combining the shear and tensile-shear fractures.

The process of rockburst evolution can be seen as a series of rock mass failure events. The relaxation or spalling of surrounding rocks caused by tensile failure only corresponds to a slight rockburst phenomena, such as rib spalling. Meanwhile, the rockbursts caused by compression-shear failures will generally result in higher intensity of the rockburst. Relevant researches have shown that the energy ratio of tensile failure is much smaller than that of shear failure. This means that if such different types of rock mass failure involved in the evolution process of rockbursts as tensile, mixed, or shear can be identified, the rockburst evolution mechanisms can be obtained directly (Xiao *et al*. 2016).

It could be seen from the aforementioned analysis of different types of rockburst phenomena occurred in the intact surrounding rock that the stress paths affects rock failure. Therefore, it is important to study the effects of stress paths for a rational stability assessment during excavation. The actual stress paths in a rock mass during excavation are complex and correctly simulate the conditions causing rockburst is important to obtain actual rock mass behavior.

3. True-triaxial test system and experimental procedure

3.1 True-triaxial system

In this study, a true-triaxial gradient and hydraulic-

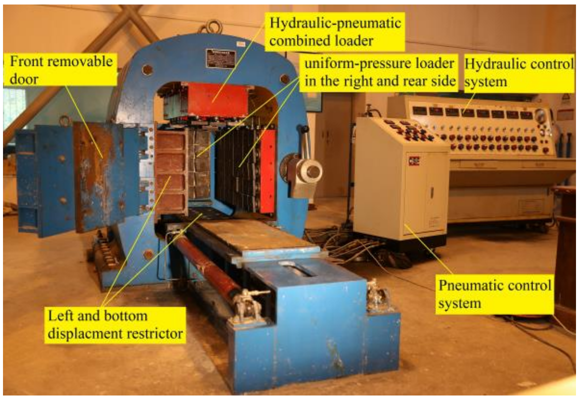

(a) Test apparatus and loading system

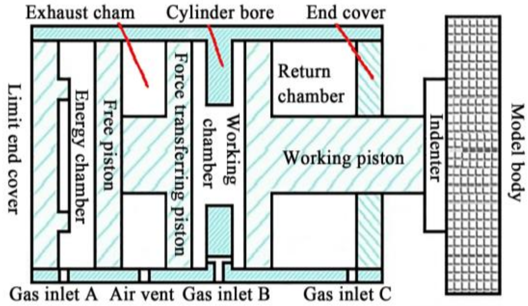

(b) Hydraulic-pneumatic combined loading device

Fig. 4 True-triaxial system

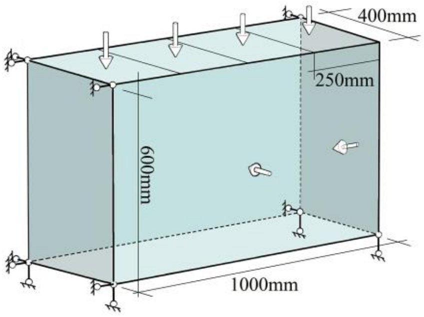

(a) Simulate the state of in-situ stress

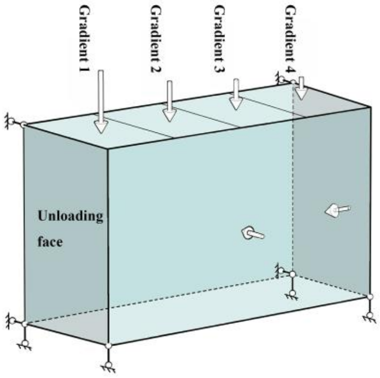

(b) Simulate excavation and tangential stress

Fig. 5 The stress state transformation of the surrounding rock masses before and after excavation

pneumatic combined text apparatus was used to perform the experiment, as depicted in Fig. 4. This novel true-triaxial testing system comprises three parts, including a main engine, a hydraulic control system, and a pneumatic control system, as shown in Fig. 4(a). The top of the main engine was equipped with four groups of independent hydraulic-pneumatic combined loading device which had a maximum loading capacity of 20MPa and could be used to load the specimen with gradient stress, as shown in Fig. 4(b). The horizontal uniform-stress loading devices with a maximum loading capacity of 5MPa were installed on the right side and the rear side of the main engine, which could realize two-dimensional and three-dimensional confining stress loading. A displacement restrictor was positioned on each face of the remaining sides.

This rockburst test apparatus could provide an exact boundary condition and stress paths for specimens during excavation. As shown in Fig. 5(a), it can realize independently three principal stress directions loading to simulate the in-situ stress state; As illustrated in Fig. 5(b), The front limit door of the device was designed to suddenly withdraw in order to expose one surface of the specimen from the true triaxial compression condition and to simulate unloading during tunnel excavations. In the meantime, the gradient stress loading at the top of the specimen simulated the tangential stress concentration processes of the rock masses during the tunnel excavation.

In most cases, the intact rock mass around the rockburst area is equivalent to a flexible loading system. Thus, when the specimen is destroyed, the stress drop of the hydraulic loading device is quickly compensated by the compression gas of the energy chamber in the hydraulic-pneumatic combined loading device, which simulates the shock effect of the strain elastic energy release of the rock mass around the rockburst area.

3.2 Selection of similar rock materials and preparation for specimen

The collection of large-scale natural specimens were restricted in practical situation, and the test was limited by the defect of the experimental apparatus. Therefore, natural rock specimens were usually replaced by similar materials.

This study mainly analyzed the rockburst characteristics under different loading paths, and mechanical parameters of the specimens were not required to meet similarity ratio. Accordingly, to make sure that the specimens were hard and brittle and also met the requirements of the loading conditions of the test apparatus, a high strength gypsum with a certain water/gypsum ratio was selected as a similar material of rock. The brittleness of the material was calibrated according to the impact energy index $W_{et} = \Phi_{sp} / \Phi_{st}$, where Φ_{sp} is the elastic strain energy accumulated prior to rock failure and Φ_{st} is the plastic strain energy consumed

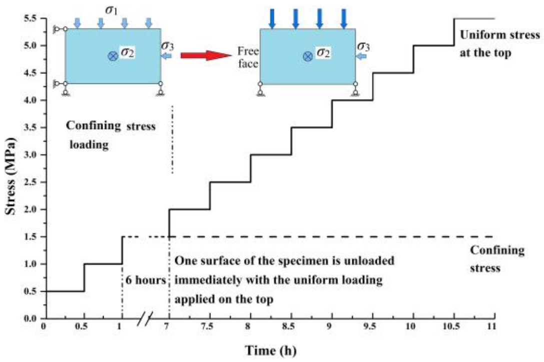

(a) b=0

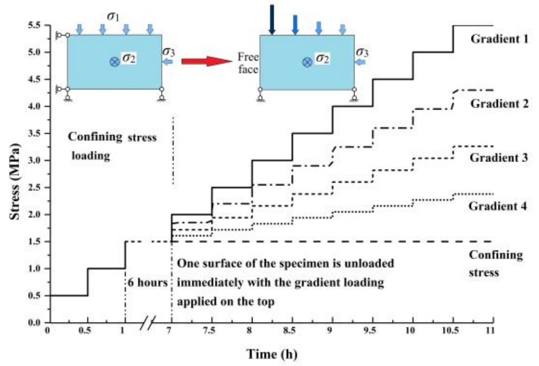

(b) b=2

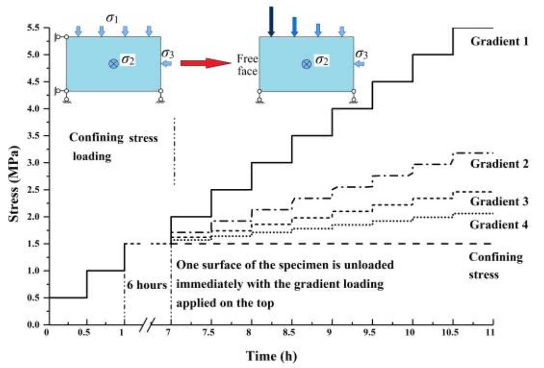

(c) b=4

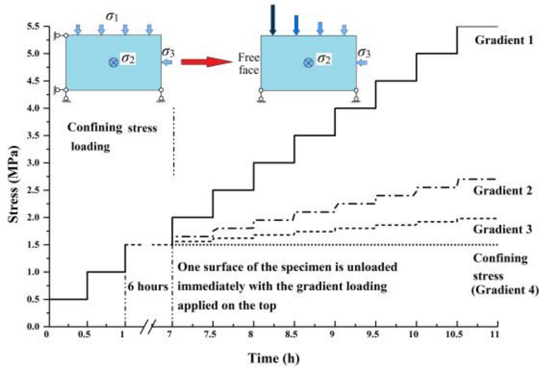

(d) b=6

Fig. 6 Test with gradient loading paths

Table 2 Specimen material parameters

Material	Water/gypsum ratio	Poisson's ratio	Young's modulus /GPa	UCS/MPa	W_{et}
Gypsum	0.6	0.25	0.334	9.2	5.8

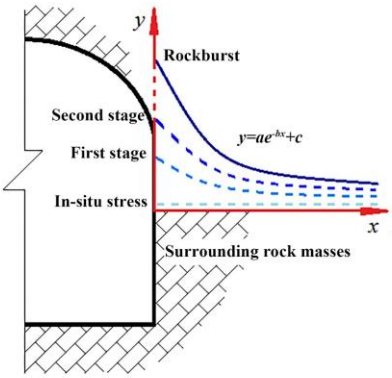

Fig. 7 Simulate the loading processes of the tangential stress in the surrounding rock masses

after rock failure. (Ghasemi *et al.* 2019). Therefore, the uniaxial compression test (UCS) was performed with different water/gypsum ratios to select the most brittle one. The specimen-related parameters are listed in Table 2. Corresponding rectangular specimens which were used for the test. Each specimen was sized at 400mm×600mm×1,000mm to meet the requirements of the testing apparatus. Meanwhile, before conducting the experiment, it should be monitored by supersonic wave to detect the integrity of the specimen and make sure the complexity of each specimen. Furthermore, to minimize the influence of lateral friction on boundary condition during loading processes, 2 layers of polymer with graphite powder were placed between each loading surface and the stress transferring platens.

3.3 Experimental procedure

This paper aims at exploring the effects of stress gradient on rockbursts. Based on the distribution laws of the tangential stress of the surrounding rock masses, the simulation of the tangential stress distributions can be simplified through the equation $y=ae^{-bx}+c$ (Singh *et al.* 2011), where y represents the tangential stress of one point inside the underground surrounding rock masses; x represents the distance from the point to the excavation boundary; $a+c$ represents the tangential stress of the excavation boundary, which is the value of gradient 1 depicted in Fig. 5(b); c represents the in-situ stress; b represents the gradient coefficient, which can reflect the gradient stress change. When b=0, the uniform stress is applied at the top of specimen; otherwise, it suffers the vertical gradient stress. It can be noted here that as b increases, the stress gradient becomes higher. In this paper, four varied gradient stress paths with *b* equaling 0, 2, 4 and 6 were designed for the loading rockburst test, corresponding to specimen #A, #B, #C, #D respectively. The concrete loading paths are plotted in Fig. 6.

According to the ratio distribution laws originated from the statistics of Brown and Hoek (1978), who collected and analyzed the in-situ stress measurement around the world, the in-situ stress for the deeply-situated rock masses can be set as hydrostatic pressure. To reduce or eliminate the end effects caused by the friction between the specimen and the platens, 1/6 of the uniaxial compression strength (viz. c=1.5 MPa) was determined as in-situ stress in this test. In the experiment, the specimens were firstly loaded with three principal stress directions. And the confining pressure was employed on each plane using step-load method, in which each loading step was 0.5 MPa. When the stress state of the loaded specimen was close to that of in-situ stress, the stress in the three principal stress directions were stabilized for 6 hours for the purpose of making the stress deformation of the specimen stable. Then the front door of the test apparatus was suddenly removed, leading to an abrupt release of stress from this plate and keeping constant the horizontal confining stress in other sides of the specimen. After simulating excavations, the AE sensors were attached respectively to different positions of the unloading face. The acoustic emission signals whose pre-amplification was at 40 dB, gain amplification at 100, and the data acquisition rate at 1 MHz. Simultaneously, the vertical stress was applied with certain gradient. Gradient 1 was still incremented by 0.5 MPa (increment of coefficient a) while other gradient stresses were calculated by $y=ae^{-b}x+c$ to be loaded synchronously until the rockburst occurred, as shown in Fig. 7. In the test, a quasi-static compact loading method was adopted. The time interval for each loading step was about 30 min, including loading and holding processes. During the test, the AE signals and the gradient loading stress of the specimens were recorded.

4. Testing results and discussion

4.1 Macroscopic damage phenomena and discussion

Rockbursts occurred in all the specimens and the specimen failure induced by the different gradient stress was captured using a conventional video camera. Fig. 8 shows the features of fragment distributions of each specimen. And the crack characteristics of the specimens after rockbursts were observed, as shown in Fig. 9. The ejection distance of the fragments and rockburst grades of specimens are listed in Table 3.

As in Fig. 8(a), the specimen #A was destroyed under the uniform loading with b=0. The fragments which were in the form of flake and thin slab were mainly distributed near the unloading face (Table 3). Seen from this, the kinetic energy of fragments was small, and the ejection process could be ignored. As presented in Fig. 9(a), the huge slabs inclined outwards, forming cracks with their opening within 1~2 cm, which were approximately paralleled to the unloading face. The slab structure was not separated from the specimen but linked with it loosely. And the surface of the slab was flat and straight without scratches. It could be seen that the specimen exhibited a typical non-dynamic spalling damage.

It could be observed from specimen #B (as shown in Fig. 8(b) and Fig. 9(b)) that as b=2, some parts of the specimen were violently exfoliated and shot out, and the fracturing phenomena were obvious, which was similar to the failure occurred in specimen #A (b=0). But the thicknesses of the the local blasting of the specimens, and the cleavage plates formed after the failure were relatively small, and the stability was weak, resulting in collapses of the splitting structures and bending outside the unloading surfaces.

As the stress gradient increased, the failure modes for specimen #C with b=4 was significantly different from those of specimen #A. It can be seen from Fig. 8(c) that the fragments which were far from the unloading face were mostly in the form of block and plate. The farthest ejection distance of these fragments was 2.7 m (Table 3), and around the larger plate fragments were the block fragments which were relatively small. It can be seen from the cracks in Fig. 9(c) that the central part of the failure plane was relatively flat and straight, presenting as tension crack faces, while the end of the cracks showed as the shear failure plane which were at an angle to the loading surface.

With the value of the *b* further increasing to 6, the specimen #D was dominated by violent failure during rockbursts, as illustrated in Fig. 8(d). Except the flake fragments near the unloading face of the specimen, a number of small blocky fragments and powders radiated away from unloading surface in the form of fan-shape. The farthest ejection distance of fragments reached 3.5 m (Table 3). This proved that the rockburst occurred in the violent manner. The propagation of the cracks from the side of the specimens presented dome-like shape, as shown in Fig. 9(d). Therefore, it can be concluded that the failure was dominated by shear sliding.

From the test results, it can be concluded that the specimens presented a variety of rockburst phenomena in different gradient stress, conforming to the rockburst phenomena in Table 1. What's more, the ejection distance of these rockburst fragments climbed from 1.0 m (b=0) to 3.5 m (b=6), which indicates that the rockburst intensities have a tendency to increase with the increase of stress gradient, as can be seen from Table 3. This proves that higher in-situ stress can cause specimen failure, but it cannot determine its mode. The rockburst under lower stress gradient presented non-violent slabbing with obvious cracks; While the rockbursts with higher stress gradient exhibited dynamic processes, and it was observed that the rockburst fragments and the specimens displayed the characterstics of the shear fracture.

The force characteristics of the rockburst failure in the specimens under different stress paths are shown in Table 4.

From the statistical results in Table 4, it can be seen that with the increases of the stress gradient, the maximum gradient stress (Gradient 1) increased gradually from 5.0 MPa (b=0) to 6.0 MPa (b=6), which suggests that the maximum gradient stress triggering the rockburst was prone to grow greater. Moreover, the ratio of the maximum gradient stress of the specimen to its uniaxial compressive strength ($\sigma_{\theta\max}/\sigma_c$) held steady at between 0.5 and 0.7, which

(a) #A (b) #B (c) #C (d) #D

Fig. 8 Distribution characteristics of fragments after rockburst of the specimens

(a) #A (b) #B (c) #C (d) #D

Fig. 9 Failure characteristics of rockbursts under different gradient stress

Table 3 The distribution statistics of specimen's fragments

Specimen	Fragment's weight/g	Mass distribution of rockburst fragments/g						Rockburst grade
		0-0.6 /m	0.6-1.0 /m	1.0-1.4 /m	1.4-1.7 /m	1.7-3.0 /m	3.5 /m	
#A	2433.3	2300	133.3	—	—	—	—	Slight
#B	2730.6	2500	220	10.6	—	—	—	Slight
#C	6565.9	2930	1620	346.7	1557.2	112	—	Medium
#D	5154.7	1340	1060	78.4	2001.6	670	4.7	Strong

Table 4 The force characteristics of the specimens when rockbursts occur

Specimen	Gradient 1 /MPa	Gradient 2 /MPa	Gradient 3 /MPa	Gradient 4 /MPa	Gradient 1/UCS
#A	5.0	5.0	5.0	5.0	0.54
#B	5.2	3.7	2.9	2.3	0.57
#C	5.5	3.0	2.0	1.7	0.59
#D	6.0	2.5	1.7	1.5	0.65

was consistent with the conclusion that the on-site rockburst was lower than its uniaxial compressive strength.

5. Analysis of rockburst characteristics

5.1 Analysis of the fragments morphology and distribution characteristics

Generally speaking, the rockburst fragments are flake, block, and grainy. In order to analyze the morphological characteristics of the fragments in this study, the length, width, and thickness of each piece of fragment were measured using vernier calipers, which were used to calculate the morphological characteristics of the fragments. The distributions of the morphological characteristics of the fragment under the different loading paths are detailed in Fig. 10. Mass ratio of fragments with different morphology are shown in Table 5. Then, in accordance with the

(a) #A (b) #B (c) #C (d) #D

Fig. 10 Failure characteristics of rockburst under different gradient stress

Table 5 Mass ratio of fragments with different morphology

Fragments morphology	Gradient stress loading paths			
	b=0	*b*=2	*b*=4	*b*=6
Flake	81.5%	70.7%	55.2%	23.5%
Block	16.2%	27.4%	43.9%	75.2%
Grainy	1.3%	1.9%	0.9%	1.3%

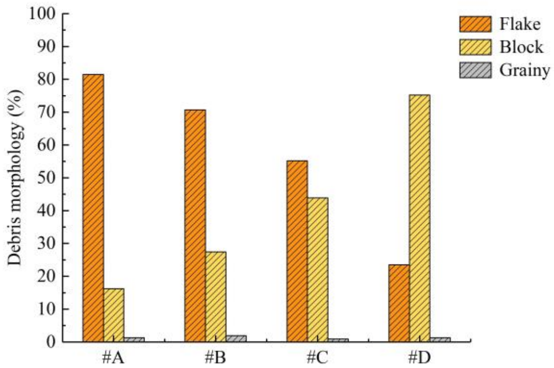

Fig. 11 Percentage distribution diagram of the fragment masses

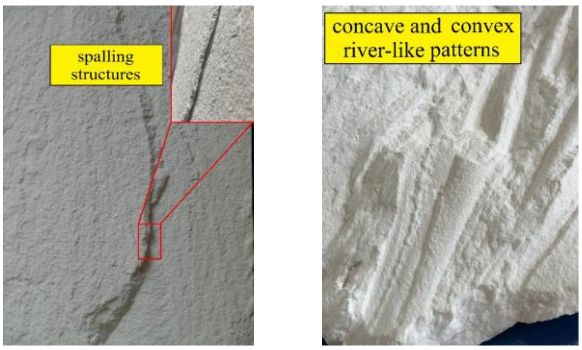

(a) Surface characteristics of the flake fragments (b) Surface characteristics of the block fragments

Fig. 12 Macroscopic surface characteristics of rockburst fragments

statistical results presented in Table 5, a percentage distribution diagram of the fragment masses was plotted in Fig. 11.

As can be seen in Table 3 and Fig. 10, under the uniform stress loading (#A, *b*=0), the percentage of the flake fragments accounts for 81.5%, while that of block fragments accounts for only 16.2%. With the increase of stress gradient, the proportion of flake fragments falls down, while the mass ratio of block fragments increased. When the stress gradient climbed up to *b*=6 (#B), the proportion of block fragments grew up to 75.2%, while that of flake fragments reduced to 23.5%. This indicates that there is a close correlation on the different types of rockburst fragments of the specimen and stress gradient, as shown in Fig.11.

5.2 Analysis of the macro-mesoscopic damage characteristics of rockburst fragments

The fragments failure modes are important features which demonstrate the failure mechanisms of rockburst. The typical fragments section morphologies during rockburst process are shown in Fig. 12. From the perspective of the section shape of the rockburst fragments, which were found to be obvious differences in the macro surface morphologies. Therefore, it was determined from the experimental results that when the stress gradient difference was large, the failure mechanisms of the simulated rockburst events were obviously different.

The macroscopic failures of material are comprehensive manifestations of many micro-cracks. In the present study, in order to obtain the micro-morphology characteristics of the fracture of block and flake fragments, the typical fragments were selected and observed using JSM-7200F thermal field emission scanning electron microscopy. However, due to the generally loose structure of the gypsum, this study chose a low magnification factor (×300) to observe the morphological features of the rockburst fragments. Fig. 13 and Fig. 14 detail the results of the fracture of flake and block fragments with scanning electron microscopy, the 3D surface reconstruction diagram and MATLAB software. Through comparative analysis, it was found that there were significant differences between the morphology and arrangement of the crystals on the mesoscopic surface of the flake and block fragments after the simulated rockburst occurred during the experiment.

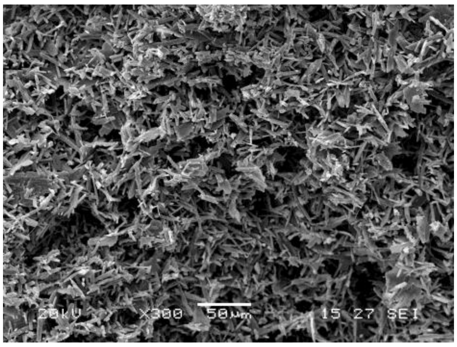

(a) SEM (×300)

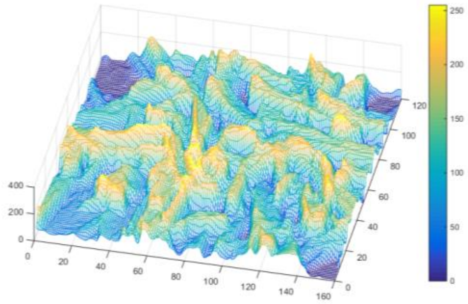

(b) Topography of 3D surface

Fig. 13 Mesoscopic surface characteristics of the flake fragments

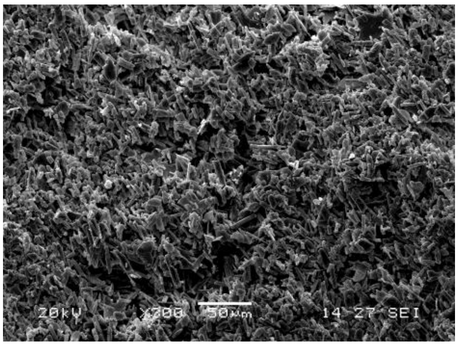

(a) SEM (×300)

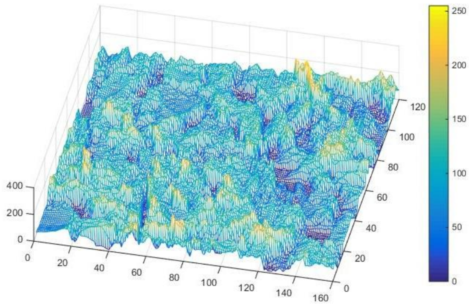

(b) Topography of 3D surface

Fig. 14 Mesoscopic surface characteristics of the block fragments

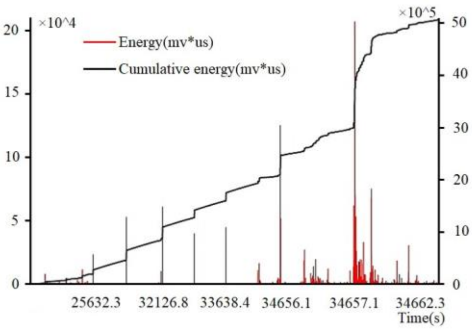

(a) #A

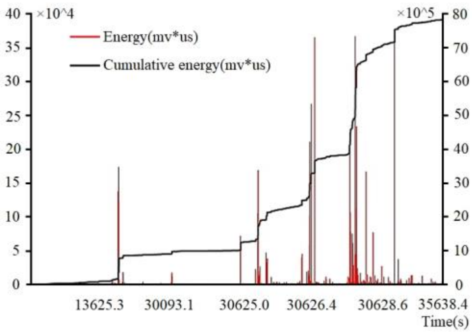

(b) #B

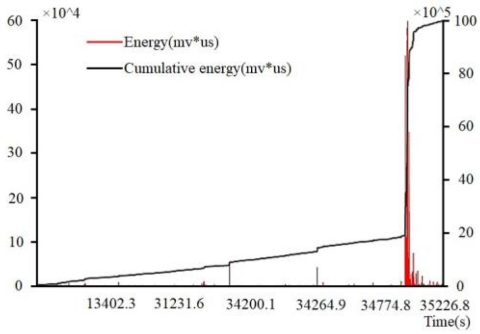

(c) #C

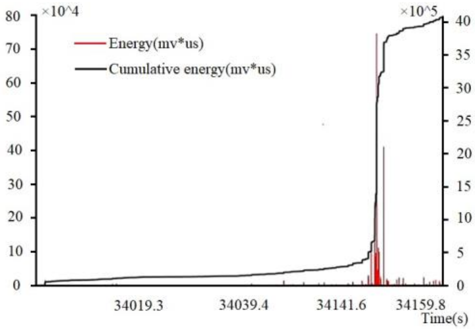

(d) #D

Fig. 15 The energy curves of the acoustic emission

Fig. 13 shows the mesoscopic surface characteristics of the flake fragments. as can be seen in Fig. 13(a) and it was found in this picture magnified up to 300 times that the cross-section was mainly composed of long columnar or needle-shaped crystals overlapping each other without directional arrangement and the surface was observed to be loose, and the crystals were relatively intact with distinct edges and corners. As can be seen from the 3D reconstruction of the clastic micro-surfaces in Fig. 13(b), the surfaces of the microcracks were undulated, in which the 3D surfaces were concave-convex and had obvious crystal contours. Fig. 14 shows the micro-surface characteristics of the block fragments. As shown in the Fig. 14(a), at a magnification of 300 times, it can be seen that the morphology of the gypsum crystal particles on the fracture surfaces was characterized by short columnar and powder-like particles, with close contact structures and relatively consistent arrangement directions for the short columnar crystals. The surfaces were blunt, and parts of the crystals had been scraped into crumbs and had filled in the gaps between the crystals. As shown in Fig. 14(b), the corresponding 3D clastic failure surfaces were relatively flat and the overall undulation was small, without complete crystal outline.

From the analysis of the brittle fracture mode of the fragments, generally, the fracture mechanism can be summarized as tensile and shear failure respectively. The microscopic section of the flake fragments was formed by tensile stress. Under the action of tensile force, the acicular crystals overlapped at the cross section and the crystal structure remained relatively intact, which was corresponding to intergranular fracture and formed a rough and loose surface structure. The straight failure path of the block fragments on the mesoscopic scale reflected the shearing processes of the fragments under loading. The gypsum crystal broke during the dislocation process of the shear section, which was corresponding to trans-granular fracture.

By macro-mesoscopic study of rockburst fragments under different loading paths, it can be found that the block fragments were produced by shear failure, while the flake fragments were produced by tensile failure. With the increase of stress gradient, the proportion of block fragments increased gradually from 16.2% (b=0) to 75.2% (b=6). It was determined that the different rockburst failure modes in the test were related to the stress loading paths. It was observed that under the loading of small stress gradient, the rockburst fragments had mainly presented intergranular tension failure (opening-mode crack), which had been dominated by flaky fragments, and its ability to accumulate energy was poor. When the simulated rockbursts occurred, there were generally no ejection phenomena produced. However, splitting and spalling were observed, which corresponded to the macroscopic failure phenomena related to flake splitting. At the same time, under the loading of large gradient stress the trans-granular shear failure (sliding-mode crack) of the rockburst was dominated by the block fragments, and the trans-granular fractures were characterized by shear displacements, which corresponded to the macroscopic failure phenomena of block shear collapse, and the corresponding rockburst intensities were moderate or even strong.

5.3 Characteristics of acoustic emission energy of rockburst under different gradient stress loading conditions

Acoustic emission phenomena can reflect much of the information contained in the specimen failure processes.

Table 6 energy parameters of the acoustic emission of the specimens

Specimens	Maximum energy/(mv*us)*10^5	Cumulative energy/(mv*us)*10^5
#A	2.07	50.65
#B	3.71	78.40
#C	5.98	99.79
#D	7.46	40.71

The brittle failure of the specimens is the result of the generation, expansion, accumulation and assembly of micro-fractures in the material, which leads to lacal weakening and in instability.

Acoustic emission energy can be used as the basis for analyzing the development of internal cracks in rock masses. Acoustic emission signals, known as the absolute energy, is not affected by the noise of the test processes, and it can satisfy a certain proportional relationship with the energy released by the material. Also, the acoustic emission signals can truly indicate the strain energy actually released by the rock specimens. The accumulated AE energy release is presented in Fig. 15 for the four rockburst types. The acoustic emission energy parameters of the specimens are shown in the Table 6.

It can be seen from the characteristics of the acoustic emission energy of Fig. 16 and Table 6 that the stress gradient was small (#A and #B); and the single acoustic emission energy was maintained at a low level during the loading processes; also, the duration was longer. With the gradient increased (#C), the initial acoustic emission energy was lower at the initial stage of the failure. The single acoustic emission energy increased significantly after loading for a period of time, indicating that the failure modes of the specimens has changed; as the stress gradient reached its maximum, the #D did not display significant energy release at the beginning of the destruction until the moment prior to the failure of the specimens, when the energy release began to accelerate and the energy accumulation curve of the acoustic emission suddenly increased, which shows the characteristics of temporal non-uniformity.

It can be concluded from the above analysis that the distribution forms of the gradient stress affect the time distributions of the energy release processes of the specimens. When the stress gradient is small, the energy release processes last for a longer time, and the corresponding energy release rates is lower. As the stress gradients increase, energy release is concentrated during the rockbursts, and the corresponding energy release rates are higher. Also, the transient characteristics are obvious. This shows that the energy release rate of rockburst increases with the rise of stress gradient.

6. Conclusions

To study the effects of different gradient stress on rockbursts, the rock-like specimens were tested through three principal stress directions loading--fast unloading of single surface--top gradient and hydraulic-pneumatic combined loading. Based on the stress states before and after excavations of deep rock masses, the rockburst characteristics occurred in underground engineering were explored. This can relatively truly simulate the failure processes of surrounding rock under the secondary stress distributions by radial stress reductions and tangential stress concentrations after the excavations of the tunnels. The following conclusions can be made based on these experimental tests results:

• The ratio of maximum gradient stress (equivalent to the maximum value of the tangential stress of the surrounding rock) to uniaxial compressive strength of the specimen material fell between 0.5 and 0.7 when rockburst occurred, which was conform to the conclusion that the tangential stress of surrounding rock is lower than the uniaxial compressive strength of the surrounding rock during rockburst. In addition, the specimen reappeared throwing phenomena. In conclusion, this test was quite similar to the rockburst occurred in the actual project, no matter seen from the simulated rockburst phenomena or from the mechanical characteristics. And this could ensure a high credibility and representativeness.

• Stress gradient of the specimens influences the rockburst grades. Seen from the ejection distance of the fragments，which climbed from 1.0 m (b=0) to 3.5 m (b=6) with the increase of stress gradient. This shows that as the stress gradient increased, the rockbursts intensities tended to be greater.

• Stress gradient influences the failure modes of specimen. When stress gradient was relatively smaller, flaky fragments accounted for 81.5%, it mainly occurred split fractures in the specimens, rockbursts tended to be progressive and static failure. While as the stress gradient increased, the proportion of blocky fragments incereased to75.2%, it mainly occurred shear-split fractures in the specimens.

• The stress gradient affects the energy release characteristics when rockburst occurs. From the perspective of characteristics of acoustic emission. As the stress gradient increased, the energy release gradually increased, and the rockburst types as well as the surrounding rock failure modes changed accordingly. This indicates that with the increase of stress gradient, rockburst gradually transited from progressive process to sudden rockburst failure.

The presented laboratory tests reveal that the stress gradient is an important factor of rockbursts. For further study, more tests with different confining pressure should be carried out to analyze their influences on rockburst phenomena.

Acknowledgments

The authors would like to sincerely thank the China Railway 12th Bureau Group Co., Ltd., as well as the China Railway Construction Group Co., Ltd., for providing the in-situ rock-burst data of the Lalin Railway Bayu Tunnel which were used in this research study. The authors would also like to express their appreciation for the financial support provided by the Research Fund for Doctoral Programs of Higher Education (No. 20110143110017); National Natural Science Foundation of China (No. 51504167); Wuhan Institute of Technology Science Fund (No. K201856); and the Fundamental Research Funds for the Central Universities (Nos. 2017-YB-022).

References

Akdag, S. Karakus, M., Taheri, A., Nguyen, G.D. and He, M.C. (2018), "Effects of thermal damage on strain burst mechanism for brittle rocks under true-triaxial loading conditions", *Rock Mech. Rock Eng*., **51**(6), 1657-1682. https://doi.org/10.1007/s00603-018-1415-3.

Brown, E.T. and Hoek, E. (1978), "Trends in relationships between measured in-situ, stresses and depth", *Int. J. Rock Mech. Min. Sci*., **15**(4), 211-215. https://doi.org/ 10.1016/0148-9062(78)91227-5.

Bruning, T., Karakus, M., Akdag, S., Nguyen, G.D. and Goodchild, D. (2018), "Influence of deviatoric stress on rockburst occurrence: An experimental study", *Int. J. Min. Sci. Technol*., **28**(5), 50-53. https://doi.org/10.1016/j.ijmst.2018.08.005.

Bruning, T., Karakus, M., Akdag, S., Nguyen, G.D. and Goodchild, D. (2018), "Experimental study on the damage evolution of brittle rock under triaxial confinement with full circumferential strain control", *Rock Mech. Rock Eng*., **51**(11), 3321-3341. https://doi.org/10.1007/s00603-018-1537-7.

Bruning, T., Karakus, M., Nguyen, G.D. and Goodchild, D. (2019), "An experimental and theoretical stress-strain-damage correlation procedure for constitutive modelling of granite", *Int. J. Rock Mech. Min. Sci*., **116**, 1-12. https://doi.org/10.1016/j.ijrmms.2019.03.003.

Cai, M. and Champaigne, D. (2012), "Influence of bolt-grout bonding on MCB conebolt performance", *Int. J. Rock Mech. Min. Sci*., **49**(1), 165-175. https://doi.org/10.1016/j.ijrmms.2011.11.006.

Diederichs, M.S., Kaiser, P.K. and Eberhardt, E. (2004), "Damage initiation and propagation in hard rock during tunnelling and the influence of near-face stress rotation", *Int. J. Rock Mech. Min. Sci*., **41**(5), 785-812. https://doi.org/10.1016/j.ijrmms.2004.02.003.

Fuławka, K., Pytel, W. and Mertuszka, P. (2018), "The effect of selected rockburst prevention measures on seismic activity-Case study from the Rudna copper mine", *J. Sustain. Min*., **17**(1), 1-10. https://doi.org/10.1016/j.jsm.2018.03.001.

Germanovich, L.N. and Dyskin, A.V. (2000), "Fracture mechanisms and instability of openings in compression", *Int. J. Rock Mech. Min. Sci*., **37**(1), 263-284. https://doi.org/10.1016/s1365-1609(99)00105-7.

Gong, Q.M., Yin, L.J., Wu, S.Y., Zhao, J. and Ting, Y. (2012), "Rock burst and slabbing failure and its influence on TBM excavation at headrace tunnels in Jinping II hydropower station", *Eng. Geol*., **124**(4), 98-108. https://doi.org/10.1016/j.enggeo.2011.10.007.

Gattinoni, P., Pizzarotti, E.M. and Scesi, L. (2014), *Engineering Geology for Underground Works*, Springer Netherlands, Milan, Italy.

Gu, J.C., Fan, J.Q., Kong, F.L., Wang, K.T., Xu, J.M. and Wang, T. (2014), "Mechanism of ejective rockburst and model testing technology", *Chin. J. Rock Mech. Eng*., **33**(6), 1081-1089 (in Chinese). https://doi.org/10.3969/j.issn.1000-6915.2014.06.001.

Ghasemi, E., Gholizadeh, H. and Adoko, A.C. (2019), "Evaluation of rockburst occurrence and intensity in underground structures using decision tree approach", *Eng. Comput*., 1-13. https://doi.org/10.1007/s00366-018-00695-9.

He, M.C., Jia, X.N., Coli, M., Livi, E. and Sousa, L. (2012), "Experimental study of rockbursts in underground quarrying of Carrara marble", *Int. J. Rock Mech. Min. Sci.*, **52**, 1-8. https://doi.org/10.1016/j.ijrmms.2012.02.006.

He, M.C., E Sousa, L.R., Miranda, T. and Zhu, G.L. (2015), "Rockburst laboratory tests database-application of data mining techniques", *Eng. Geol.*, **185**, 116-130. https://doi.org/10.1016/j.enggeo.2014.12.008.

Hauquin, T., Gunzburger, Y. and Deck, O. (2018), "Predicting pillar burst by an explicit modelling of kinetic energy", *Int. J. Rock Mech. Min. Sci.*, **107**, 159-171. https://doi.org/10.1016/j.ijrmms.2018.05.004.

Ptáček, J. (2017), "Rockburst in ostrava-karvina coalfield", *Procedia Eng.*, **191**, 1144-1151. https://doi.org/10.1016/j.proeng.2017.05.289.

Li, T., Ma, C., Zhu, M., Meng, L. and Chen, G. (2017), "Geomechanical types and mechanical analyses of rockbursts", *Eng. Geol.*, **222**, 72-83. https://doi.org/10.1016/j.enggeo.2017.03.011.

Mazaira, A. and Konicek, P. (2015), "Intense rockburst impacts in deep underground construction and their prevention 1", *Can. Geotech. J.*, **52**(10), 1426-1439. https://doi.org/10.1139/cgj-2014-0359.

Manouchehrian, A. and Cai, M. (2016), "Simulation of unstable rock failure under unloading conditions", *Can. Geotech. J.*, **53**(4), 22-34. https://doi.org/10.1139/cgj-2015-0126.

Qiu, S.L., Feng, X.T., Zhang, C.Q. and Xiang, T.B. (2014), "Estimation of rockburst wall-rock velocity invoked by slab flexure sources in deep tunnels", *Can. Geotech. J.*, **51**(5), 520-539. https://doi.org/10.1139/cgj-2013-0337.

Roohollah, S.F. and Abbas, T. (2018), "Long-term prediction of rockburst hazard in deep underground openings using three robust data mining techniques", *Eng. Comput.*, **35**(2), 659-675. https://doi.org/10.1007/s00366-018-0624-4.

Singh, A.K., Singh, R., Maiti, J., Kumar, R. and Mandal, P.K. (2011), "Assessment of mining induced stress development over coal pillars during depillaring", *Int. J. Rock Mech. Min. Sci.*, **48**(5), 805-818. https://doi.org/10.1016/j.ijrmms.2011.04.004.

Stacey, T.R. (2016), "Addressing the consequences of dynamic rock failure in underground excavations", *Rock Mech. Rock Eng.*, **49**(10), 4091-4101. https://doi.org/10.1007/s00603-016-0922-3.

Song, D.Z., Wang, E.Y., Li, Z.H., Qiu, L.M. and Xu, Z.Y. (2017), "Emr: an effective method for monitoring and warning of rock burst hazard", *Geomech. Eng.*, **12**(1), 53-69. https://doi.org/10.12989/gae.2017.12.1.053.

Tan, Y.L., Liu, X.S. Shen, B., Ning, J.G. and Gu, Q.H. (2018), "New approaches to testing and evaluating the impact capability of coal seam with hard roof and/or floor in coal mines", *Geomech. Eng.*, **14**(4), 367-376. https://doi.org/10.12989/gae.2018.14.4.367.

Wang, C.L., Chuai, X.S., Shi, F., Gao, A.S. and Bao, T.C. (2018), "Experimental investigation of predicting rockburst using Bayesian model", *Geomech. Eng.*, **15**(6), 1153-1160. https://doi.org/10.12989/gae.2018.15.6.1153.

Xiao, Y.X., Feng, X.T., Li, S.J., Feng, G.L. and Yu, Y. (2016), "Rock mass failure mechanisms during the evolution process of rockbursts in tunnels", *Int. J. Rock Mech. Min. Sci.*, **83**, 174-181. https://doi.org/10.1016/j.ijrmms.2016.01.008.

Yan, P., Zhao, Z., Lu, W., Fan, Y., Chen, X.R. and Shan, Z.G. (2015), "Mitigation of rock burst events by blasting techniques during deep-tunnel excavation", *Eng. Geol.*, **188**(1), 126-136. https://doi.org/10.1016/j.enggeo.2015.01.011.

JS